Collaborative RF-SLAM for Multipath Channels

Robert M. Tenny, Todd E. Humphreys, *The University of Texas at Austin* Atieh Khamesi, Thomas Cheng, Stefan Adalbjörnsson *Ericsson Research*

BIOGRAPHY

Robert M. Tenny Robert Tenny is a Ph.D. student in the department of Electrical and Computer Engineering at The University of Texas at Austin and a member of the Radionavigation Laboratory. He earned his BS, Electrical Engineering, University of Kansas and MS, Electrical Engineering, University of Texas at Austin. His work focuses on robust navigation systems for urban air mobility, autonomous vehicles, and extended reality. His research interests include signal processing, sensor fusion, SLAM, and joint communications and sensing.

Atieh R. Khamesi Dr. Atieh R. Khamesi earned her Ph.D. in Information Engineering from the University of Padova, Italy, in 2018. She was a Visiting Scholar at Virginia Tech and a Postdoctoral Scholar at the University of Kentucky, focusing on cyber–physical–human systems. At Ericsson Research in Santa Clara, CA, she applies machine learning, optimization, and algorithm design to intelligent localization and wireless communications, and has led the 3GPP Release 19 feature on AI for air interface positioning

Thomas Cheng Jung-Fu (Thomas) Cheng is a Principal Researcher at Ericsson Research Silicon Valley. His research interests include channel coding, MIMO signal processing, spectrum sharing, and applications of ML techniques to wireless systems. Dr. Cheng holds over 400 US patents and was named Ericsson Inventor of the Year in 2012. He was a co-recipient of IEEE Communications Society Leonard G. Abraham Prize Paper Award.

Stefan Adalbjörnsson Stefan Adalbjörnsson is a Research Leader at Ericsson Research, Austin, TX, USA. He received the Ph.D. in mathematical statistics from Lund University, Sweden. His work spans AI/ML, data science, and statistical signal processing for telecom and radar, emphasizing algorithm—hardware co-design and efficient ASIC/accelerator implementations. Contributions include AI rApps for RAN optimization, vision-based positioning/tracking, and high-accuracy radar localization. He has authored more than 40 peer-reviewed publications and is the inventor on 4 granted patents and over a dozen patent applications.

Todd E. Humphreys Todd E. Humphreys holds the Ernest Dashiell Cockrell II Chair in Engineering in the department of Aerospace Engineering and Engineering Mechanics at The University of Texas at Austin. He is Director of the Wireless Networking and Communications Group and of the UT Radionavigation Laboratory. He specializes in the application of optimal detection and estimation techniques to problems in secure, collaborative, and high-integrity automated situational awareness. His publications are among the most cited in the field of positioning, navigation, and timing. His awards include the National Science Foundation CAREER Award (2015), the Institute of Navigation Thurlow Award (2015), the IEEE Walter Fried Best Paper Award (2012, 2020, 2023), the Presidential Early Career Award for Scientists and Engineers (PECASE, via NSF, 2019), the Institute of Navigation Kepler Award (2023), and the Royal Institute of Navigation. He earned his B.S. and M.S. in Electrical and Computer Engineering from Utah State University, and his Ph.D. in Aerospace Engineering from Cornell University.

ABSTRACT

This paper presents a collaborative technique for radio-frequency simultaneous localization and mapping (RF-SLAM) for positioning in indoor environments and urban canyons using signals from a single base station. Multipath effects in indoor environments and urban canyons create ambiguities in both the time of arrival (TOA) and angle of arrival (AOA) measurements, causing difficulty for traditional localization methods. Yet reflections can be exploited for positioning by serving as landmarks for RF-SLAM. Multipath components caused by specular reflections are used to aid in positioning by estimating the location of a virtual transmitter (VT) transmitting a signal with the same properties as the reflected signal. The line-of-sight path to the base station and specular reflections are used to jointly estimate the user's position, velocity, and the position of VTs, enabling robust positioning despite multipath channels. This paper makes three primary contributions. First, it develops the unscented Poisson multi-Bernoulli mixture SLAM (UPMBM-SLAM) estimator to tightly couple TOA and AOA measurements with an inertial sensor to jointly estimate the UE and VT positions and detect walls. Second, it validates the UPMBM-SLAM estimator using data simulated by ray tracing software. Third, it leverages the VT estimates from multiple UEs to create collaborative maps of the VT locations and thereby improve localization precision.

I. INTRODUCTION

New standards such as 5G NR provide positioning services for user equipment (UE) [Dwivedi et al., 2021]. Robust UE positioning is essential for emerging technologies such as immersive open-world extended reality [Humphreys et al., 2020, Tenny et al., 2023], autonomous vehicles [Wymeersch et al., 2017] and improved network performance [Koivisto et al., 2017]. The current positioning techniques for 5G NR rely on line-of-sight (LOS) channels in order to achieve best performance [Yang et al., 2022].

Traditional radio-frequency-based localization techniques require LOS signals from multiple base stations (BSs) for time of arrival (TOA) measurements or a single LOS signal from a single BS with both TOA and angle of arrival (AOA) measurements for localization. However, a UE in urban environments will likely only have a strong signal from a single BS with a several multipath components (MPCs) created by the signal reflecting off of surfaces in the environment causing ambiguity in both TOA and AOA measurements. Each MPC contains potentially useful information about the geometry of the environment that can be exploited for positioning.

Existing techniques for localization in multipath channels can be divided into two main categories, fingerprinting and radio frequency simultaneous localization and mapping (RF-SLAM). A fingerprinting approach relies on a high-fidelity map of channel information at known positions to build a map of the received signal properties such as a spectrogram, TOA, AOA, or other measurements derived from the received signal [Wu et al., 2022]. The UE position is then determined by correlating received signal properties at the unknown UE position with the map. Fingerprinting techniques are often implemented using machine learning models trained using the map of received signal properties at known UE positions. The trained model is able to infer the UE's position from the received signal properties [Gao et al., 2022] with sub-meter or even sub-decimeter precision. The primary drawback of fingerprinting is the requirement to create maps over an entire coverage area, placing a burden on map makers to create and update maps within which each survey point's location and channel information are precisely known. Fingerprinting methods have the additional drawback inability to be adapted to new environments.

RF-SLAM exploits MPCs created by specular reflections. The specular MPCs arise due to reflections off surfaces in the environment. These create an image of the BS that can be modeled as a virtual transmitter (VT) [Gentner et al., 2016]. A VT represents a transmitter with the properties necessary to generate a signal that is indistinguishable from a MPC. The VT positions serve as references in an RF-SLAM architecture where the location of the UE and VTs are jointly estimated. The process of leveraging specular reflections for RF-SLAM has been extensively studied in the literature. RF-SLAM methods based on belief propagation, such as BP-SLAM [Leitinger et al., 2019, Kim et al., 2023, Yang et al., 2021], are able to jointly estimate a UE position and multiple VT positions and estimate the *a priori* probability distributions of VTs. However, BP-SLAM assumes a fixed vector of VTs without a method for handing real world effects such as not knowing the number of VTs *a priori* and disappearing VTs caused by finite-length reflectors.

The limitations of belief propagation can be solved by modeling the set of VTs as a random finite set (RFS). A RFS of VTs considers both the VT positions, and the cardinality of the set of VTs as unknown, enabling it to accurately model a set of VTs [García-Fernández et al., 2021]. The difficulty in modeling the set of VTs and estimating their locations is the measurement association problem. At a given timestep, a set of TOA and AOA measurements is generated by receiving a signal interacting with a multipath environment. The TOAs and AOAs are generated by both the line-of-sight path to the BS and specular reflections that can be modeled as originating from VTs. In addition, there are TOAs and AOAs that arise due to MPCs causes by diffuse reflections and diffraction paths which can not be modeled by VTs. Each measurement, whether caused by a diffuse or specular reflection, must be associated with the correct VT, BS, or no VT to correctly estimate the UE and VTs positions. In the literature an RFS is modeled by a position multi-Bernoulli mixture (PMBM) [García-Fernández et al., 2018] to solve the measurement association problem. PMBM-based techniques have been demonstrated for mmWave localization [Ge et al., 2022, Kim et al., 2022]. Prior PMBM-based techniques have been focused on vehicular networks [Kim et al., 2022] and do not incorporate measurements from inertial sensors. The EK-PMBM filter [Ge et al., 2022] provides a computationally efficient method of estimating the UE position, but it does not track the VT position. This causes the EK-PMBM estimator to rely completely on the initial estimates of the VT locations, which means any errors in the estimated VT position will not be corrected. In addition, the EK-PMBM estimator is not coupled with an inertial sensor and does not account for UE clock drift when modeling the UE clock.

This paper presents the Unscented Poisson Multi-Bernoulli Mixture SLAM (UPMBM-SLAM) estimator for RF-SLAM. The UPMBM-SLAM estimator jointly estimates the UE position, velocity, clock bias, and VT positions by tightly integrating a PMBM estimator employing the unscented transform with inertial sensor measurements. In addition, the UPMBM-SLAM estimator incorporates a two-parameter clock model for improved timing performance. The map of VT positions resulting from RF-SLAM serves as a high-confidence *a priori* map for neighboring UEs and is collaboratively updated. In addition, the maps of VTs allow for the UE to detect walls or other reflectors in the environment. The same VT locations provide knowledge of the MPC of the channel, allowing future users to leverage the prior knowledge about the channel to improve communications reliability.

This paper makes three primary contributions. First it introduces the UPMBM-SLAM estimator, which tightly couples channel estimates with an inertial sensor to jointly estimate the UE and VT positions and detect walls. Second, it evaluates the UPMBM-SLAM estimator performance using data simulated by ray tracing software. Third, it introduces collaborative UPMBM-SLAM, which exploits multiple UEs to create collaborative maps of the VT locations, and demonstrates improvements in the localization performance that such a collaborative scheme offers.

II. UPMBM-SLAM OVERVIEW

The MPCs detected by the UE receiver are due to the multipath response of the channel. Each MPC can be due to the line-of-sight path, specular reflection, diffuse reflection, diffraction path, scattering, or other multipath effects. The goal of the UPMBM-SLAM filter is to jointly estimate the UE state and VTs' locations using TOA and AOA measurements of the MPCs as shown in Fig. 1. Tracking the locations of the VTs from TOA and AOA measurements is similar to the multi-target tracking (MTT) problem faced by a radar receiver detecting and tracking multiple targets. The UPMBM-SLAM estimator is built on a Poisson multi-Bernoulli mixture (PMBM) filter. The PMBM filter [García-Fernández et al., 2018] provides a method of MTT by modeling the set of VTs as a random finite set (RFS) enabling both the location of multiple VTs to be estimated and the cardinality of the set of VTs.

The RFS of VT positions is a set **X** where the cardinality of the set is a random variable. The probability density of the set **X** is a weighted mixture of a Poisson point process (PPP) representing the VTs that have not been detected, and a multi-Bernoulli mixture (MBM) of the detected VTs [García-Fernández et al., 2018]. When the UE is first initialized, it only has knowledge of the true BS location and a model for the PPP representing the birth model for undetected VTs. The MBM component models the set of detected VTs with a set of weighted global hypotheses. Each global hypothesis represents a realization of **X** and each component of the global hypothesis is a singe VT with a Bernoulli probability of exiting. Initially the full RFS of VTs **X** is contained by a single PPP with mean at the location of the known BS but the weight of the PPP decreases as more VTs are detected and more MBM components are generated.

The PMBM has the benefit of not requiring labeling the measurements or VTs, allowing the filter to be initialized with minimal prior knowledge of the environment in the form of the PPP describing the birth model of VTs. In the RF-SLAM problem the measurements of MPCs may be in an arbitrary order due to position of the UE relative to reflectors in the environment. A PMBM-based estimation method can estimate the RFS **X** despite these challenges. The details of the data association will be discussed in more detail in the following sections.

III. SYSTEM MODEL

This section outlines the measurement and dynamics models used in the UPMBM-SLAM estimator.

1. Estimator State

The UPMBM-SLAM estimator jointly tracks the UE and VT states. The UE state is defined as containing the UE position $\mathbf{x} \in \mathbb{R}^3$, velocity $\dot{\mathbf{x}} \in \mathbb{R}^3$, and local clock offset δt :

$$\boldsymbol{X}_{\mathrm{u}}(k) = [\boldsymbol{x}(k), \dot{\boldsymbol{x}}(k), \delta t(k)]^{\mathsf{T}}$$

The state describing positions of the detected VTs contains the position of the i^{th} VT, $\mathbf{x}_i \in \mathbb{R}^3$, for i = 1, ..., n:

$$\boldsymbol{X}_{\text{vt}}(k) = [\boldsymbol{x}_1(k), \boldsymbol{x}_2(k), \dots, \boldsymbol{x}_n(k)]^{\mathsf{T}}$$
(1)

The state \mathbf{X}_{vt} represents a single realization of a RFS of VTs. The cardinality of \mathbf{X}_{vt} may be different for each hypothesis and at each timestep due to the number of VTs detected. Each hypothesis \mathbf{h} is defined as:

$$\mathbf{h}(k) = {\mathbf{X}_{vt}(k), w_1(k), \dots, w_i(k)}$$

where the i^{th} VTs in the hypothesis is described by a Bernoulli weight w_i to model its probability of existing, i = 1, ..., n. More details about the multi-hypothesis modeling are presented in Section IV.

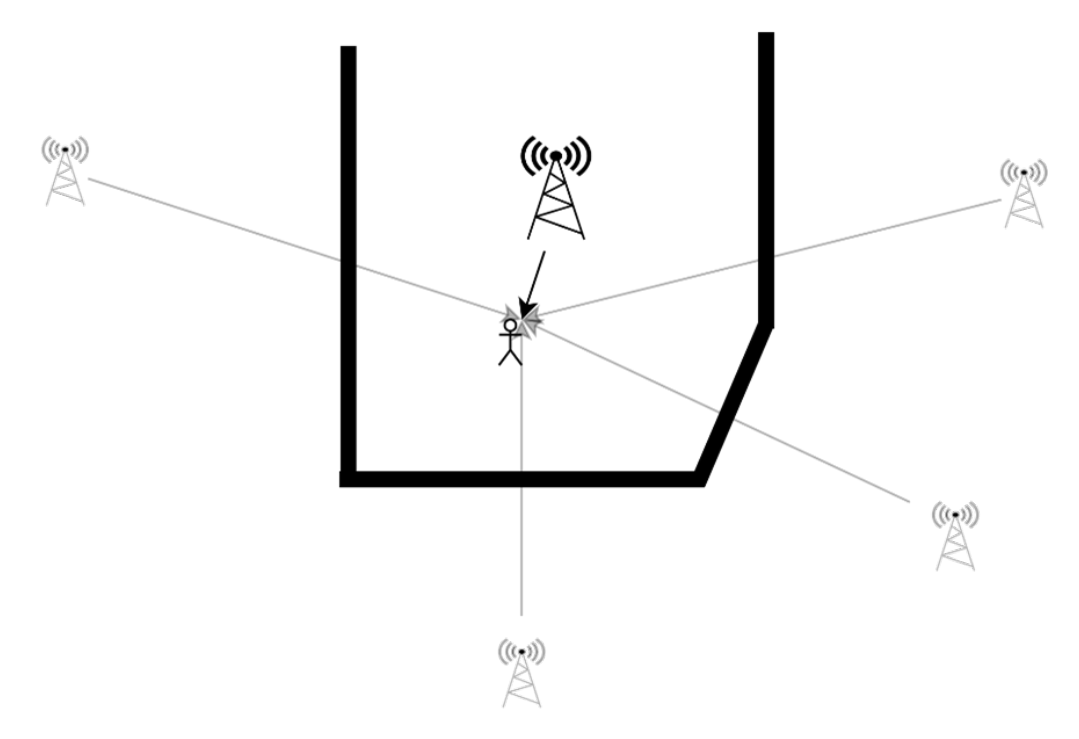


Figure 1: Sketch showing the VTs that result from specular reflections of the BS signal off walls in the environment. The large opaque transmitter in the center represents the known BS location while the grey transmitters are the VTs that model signals created by specular reflections of the BS signal. The multipath components of the signal environment can be equivalently modeled as being line of sight signals originating from VTs.

2. Measurement Models

During the process of communicating with the BS the UE is continuously estimating the channel parameters to both improve communications and for positioning [Dwivedi et al., 2021]. Parameters such as the signals time of arrival (TOA) and angle of arrival (AOA) can be measured from the received signal and used to estimate the position of the UE. For scheduled communications with a known transmit time a signals time of flight (TOF) can be found from the difference between the TOA and the transmit time. It is assumed that the transmitter clock at the BS is well characterized and disciplined by a Global Navigation Satellite System [Ruffini et al., 2021]. The TOFs can be multiplied by the speed of light c to create pseudorange measurements. The pseudorange $\rho_i(k)$ of the i^{th} MPC at time k is modeled as a function of the Euclidean distance between the i^{th} VT location \mathbf{x}_i and the UE location \mathbf{x}_u , the clock offset δt , and additive white Gaussian measurement noise \mathbf{w}_i^p .

$$\rho_i(k) = c\delta t(k) + \|\mathbf{x}_i(k) - \mathbf{x}_{\mathbf{u}}(k)\| + \mathbf{w}_i^{\rho}(k)$$
(2)

The AOA measurement corresponding to MPC i at time k consist of an azimuth angle θ_i and elevation angle ϕ_i . The AOAs are modeled as a function of the unit direction vector from the UE to the VT $\mathbf{d} = [d_x, d_y, d_z]^\mathsf{T}$ and additive noise component w^θ and w^ϕ :

$$\theta_n(k) = \arctan\left(\frac{d_y}{d_x}\right) + w_i^{\theta}(k)$$
 (3)

$$\phi_i(k) = \arctan\left(\frac{d_z}{\sqrt{d_x^2 + d_y^2}}\right) + w_i^{\phi}(k) \tag{4}$$

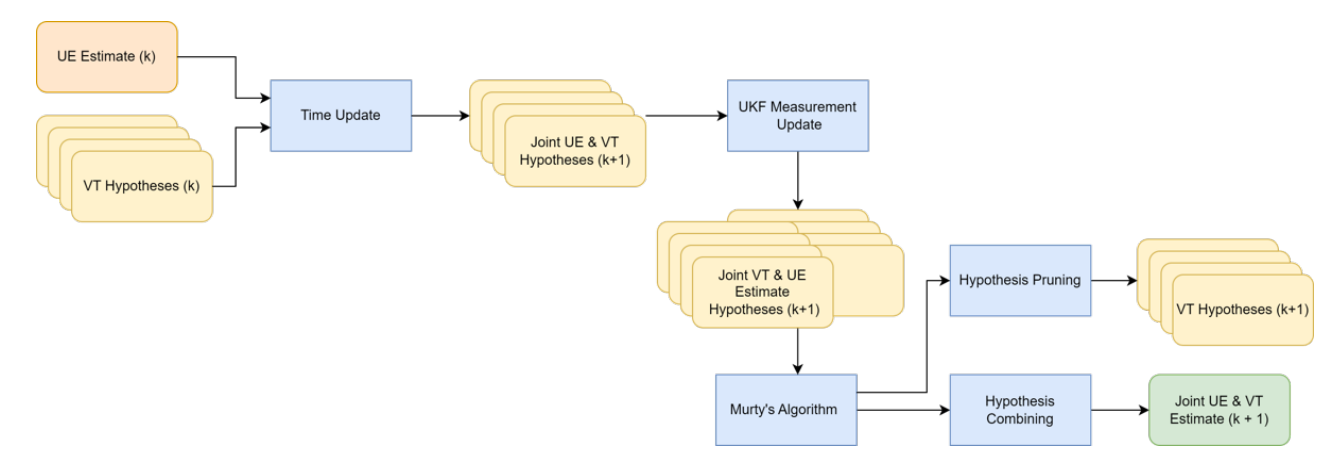


Figure 2: Block diagram of UPMBM-SLAM estimator's structure. The orange box represents the initial state and the green box represents the filtered output of the estimator. The yellow and orange boxes represent the internal states of the estimator and the blue boxes represent operations performed on the states.

The noise components w^{θ} and w^{ϕ} are assumed to be mutually uncorrelated and von Mises fisher distributed.

3. Dynamics Model

The UE dynamics are modeled by directly integrating specific force measurements from an inertial sensor over a timestep Δt . The dynamics include process noise $\mathbf{v}_{\mathrm{u}}(k)$ which represents both the noise due to errors in the specific force measurements, clock errors, and any other errors caused by processes not modeled by the dynamics.

$$\boldsymbol{X}_{\mathrm{u}}(k+1) = \boldsymbol{f}[\boldsymbol{X}(k), \boldsymbol{u}(k), \boldsymbol{v}_{\mathrm{u}}(k)] \tag{5}$$

Where the vector \boldsymbol{u} holds the IMU angular rate $\tilde{\boldsymbol{\omega}}$ and specific force $\tilde{\boldsymbol{f}}$ measurements:

$$\boldsymbol{u}(k) = [\tilde{\boldsymbol{\omega}}(k), \tilde{\boldsymbol{f}}(k)]^{\mathsf{T}}$$

and v_{ij} holds the process noise elements,

$$\mathbf{v}_{u}(k) = [\mathbf{v}_{g}(k), \mathbf{v}_{g2}(k), \mathbf{v}_{a}(k), \mathbf{v}_{a2}(k), \mathbf{v}_{\delta t}(k)]^{\mathsf{T}}$$

$$(6)$$

The process noise vector $\mathbf{v}_u(k)$ is modeled as zero mean, uncorrelated in time and having covariance matrix Q(k) and independent of the measurement noise $\mathbf{\omega}(k)$ and state \mathbf{X}_u :

$$\mathbb{E}\left[\mathbf{v}_{\mathbf{u}}(k)\mathbf{v}_{\mathbf{u}}(k)^{\mathsf{T}}\right] = 0$$

$$\mathbb{E}\left[\mathbf{v}_{\mathbf{u}}(k)\mathbf{v}_{\mathbf{u}}(j)^{\mathsf{T}}\right] = Q(k)\boldsymbol{\delta}_{kj}$$

$$\mathbb{E}\left[\mathbf{v}_{\mathbf{u}}(k)\boldsymbol{\omega}(j)^{\mathsf{T}}\right] = 0\forall k, j$$

$$\mathbb{E}\left[\mathbf{X}_{\mathbf{u}}(k)\mathbf{v}_{\mathbf{u}}(j)^{\mathsf{T}}\right] = \mathbb{E}\left[\mathbf{X}_{\mathbf{u}}(k)\right]\mathbb{E}\left[\mathbf{v}_{\mathbf{u}}(j)\right]$$

The process noise is drawn from the IMU measurement model and the clock process noise is defined by the covariance of the clock offset. Where $\sigma_{\delta t}^2$ is the covariance of the clock offset. The dynamics model the clock offset δt as a constant value with covariance [Brown and Hwang, 2012]:

$$\sigma_{\delta t}^{2} = \left(\frac{h_{0}}{2}\Delta t + 2h_{-1}\Delta t^{2} + \frac{2}{3}\pi^{2}h_{-2}\Delta t^{3}\right)c^{2}$$

Where the parameters h_0 , h_{-1} , and h_{-2} are found from the Allen deviation of the UE clock [Brown and Hwang, 2012].

The time interval Δt is considered small enough that the discrete-time function $\mathbf{X}_{\mathrm{u}}(k+1) = \mathbf{f}[\mathbf{X}(k), \mathbf{u}(k), \mathbf{v}_{\mathrm{u}}(k)]$ can be implemented using Euler integration. The values of $\mathbf{u}(k)$ and $\mathbf{u}_{\mathrm{u}}(k)$ are assumed to be constant for the short Δt . Then \mathbf{f} is modeled as:

$$\begin{bmatrix} \boldsymbol{x}(k+1) \\ \dot{\boldsymbol{x}}(k+1) \\ \delta t(k+1) \\ \boldsymbol{e}(k+1) \\ \boldsymbol{b}_{a}(k+1) \\ \boldsymbol{b}_{g}(k+1) \end{bmatrix} = \begin{bmatrix} \boldsymbol{x}(k) + \Delta t \dot{\boldsymbol{x}}(k) + \frac{1}{2}(\Delta t)^{2}\boldsymbol{a}(k) \\ \dot{\boldsymbol{x}}(k) + \Delta t \boldsymbol{a}(k) \\ \delta t(k) + \Delta t \\ \boldsymbol{e}(k) + \Delta t \dot{\boldsymbol{e}}(k) \\ \alpha_{a}\boldsymbol{b}_{a}(k) + \boldsymbol{v}_{a2}(k) \\ \alpha_{g}\boldsymbol{b}_{g}(k) + \boldsymbol{v}_{g2}(k) \end{bmatrix} = \boldsymbol{f}[\boldsymbol{X}(k), \boldsymbol{u}(k), \boldsymbol{v}_{u}(k)]$$

The state and dynamics function are simplified in this case by assuming that the bias \boldsymbol{b}_g and \boldsymbol{b}_a parameters of the IMU are known and well characterized allowing them to be removed from the sate. In addition, the orientation of the UE is not tracked an the orientation \boldsymbol{e} is removed from the sate to simplify the model.

The VTs are considered to be stationary and are modeled according to the dynamics below:

$$\boldsymbol{X}_{\text{vt}}(k+1) = \boldsymbol{F}_{\text{vt}}\boldsymbol{X}_{\text{vt}}(k) + \boldsymbol{v}_{\text{vt}}(k) \tag{7}$$

The state transition matrix F_{vt} is defined as I_{3n} where n is the cardinality of the RFS of VTs. The process noise v_{vt} is modeled as having the covariance $Q_{vt}(k)$ is a $3n \times 3n$ matrix where n is the number of visible VTs at time k:

$$\mathbb{E}\left[\boldsymbol{\nu}_{\text{vt}}(k)\boldsymbol{\nu}_{\text{vt}}(k)^{\mathsf{T}}\right] = \boldsymbol{Q}_{\text{vt}}(k) \tag{8}$$

IV. ESTIMATOR STRUCTURE

The UPMBM-SLAM estimator has its primary structure based on a MTT-PMBM filter [García-Fernández et al., 2018, Ge et al., 2022, Kim et al., 2022] with modifications to allow for the joint estimation of the UE states, VT states, and coupling with an accelerometer (Fig. 2).

1. Time Update

a) UE Time Update

The first step in the UPMBM-SLAM filter is the time update. The filter propagates the prior best estimate of the UE state at time k to time k+1 following the dynamics model shown in (5) where the state transition matrix \mathbf{F}_u is found from the dynamics function shown in (5). The UE state is updated according to the IMU measurements taken from an accelerometer at time k If the measurement rate of the inertial sensor is sufficiently high the errors from Euler integration of the specific force measurements will be negligible. After the time update the augmented UE state is pruned down to only the UE state shown in (5). The UE state error covariance is propagated through the square of the linear dynamics with an additive process noise covariance \mathbf{Q}_u is shown in (6).

$$\bar{\boldsymbol{P}}_{\mathrm{u}}(k+1) = \boldsymbol{F}_{\mathrm{u}}\boldsymbol{P}_{\mathrm{u}}(k)\boldsymbol{F}^{\mathsf{T}} + \boldsymbol{Q}_{\mathrm{u}}(k)$$

b) PMBM Time Update

At each timestep the the PMBM consists of a weight w_p on the PPP representing undetected VTs and clutter and the MBM components represented by a maximum of γ hypotheses. At each timestep the weight on the PPP w_p is updated and the VT locations in each MBM hypothesis are updated. When The UPMBM-SLAM estimator is initialized with either an empty prior hypothesis defined as an empty set and $w_p = 1$, or with a single *a priori* hypothesis representing a prior map and w_p .

Each hypothesis represents a RFS of VTs defined according to (1). Each hypothesis is updated with a linear update according to the dynamics shown in (7) as shown below:

$$\begin{split} \bar{\boldsymbol{X}}_{\text{vt}}(k+1) &= \boldsymbol{F}_{\text{vt}}\hat{\boldsymbol{X}}_{\text{vt}}(k) \\ \bar{\boldsymbol{P}}_{\text{vt}}(k+1) &= \boldsymbol{F}_{\text{vt}}\boldsymbol{P}_{\text{vt}}(k)\boldsymbol{F}^{\mathsf{T}} + \boldsymbol{Q}_{\text{vt}}(k) \end{split}$$

Where \mathbf{F}_{vt} is the identity matrix I_{3n} where n is the cardinality of the RFS. The VTs' states are modeled as being constant resulting in the state transition matrix being multiplication with the identity matrix. The process noise shown in (8) is additive and Gaussian with covariance matrix equal to the block diagonal of the VT error covariance σ_{vt}^2 .

The PPP weight w_p , representing the weight of the undetected VTs, is updated each time step to account for the VTs that have already been detected.

$$w_{\rm p}(k+1) = (1 - P_{\rm d}(k))w_{\rm p}(k) \tag{9}$$

where, P_d is the detection probability. The Poisson weight continues to decay each timestep based upon the detection probability which describes the probability of detecting a VT at each timestep. The detection probability can be tuned based on the density of VTs in an environment. For example one can expect the detection probability to be larger in an urban environment with lots of reflecting surfaces compared to a suburban or rural environment. If the Poisson weight falls below a threshold ε the value of w_p is set equal to ε to model the undetected VTs will become visible in the future. If the UE is exploring an unbounded environment, it is necessary to allow for new VTs to be detected as new reflecting surfaces come into view resulting in new VTs to appear and are subsequently tracked by the filter.

2. Measurement Update

The UPMBM-SLAM filter tracks the MBM components using multiple hypotheses. Each hypothesis contains a RFS of VTs and the corresponding UE state. Each hypothesis in the MBM components are used to account for each possible data association between the VTs and MPCs in addition to the case that a measurement is from a previously undetected VT or not due to a VT. The measurement update step consists of generating a hypothesis for each combination of prior VT hypothesis with each possible measurement and evaluating the likelihood of the combinations.

For the measurement update at time k + 1 each measurement is initially considered to represent an undetected VT and a joint UE and VT UKF measurement update is performed using the measurement models shown in (2, 3, 4). The distribution of the distribution of the PPP is used as the *a priori* distribution of the VT location and the *a priori* distribution of the UE position is a Gaussian distribution with mean and covariance found from the time update step. An augmented state is created by combining the UE state with the *n* VT states. The *k*'s have been suppressed for readability in this section for clarity.

$$\boldsymbol{\bar{X}}_a = [\boldsymbol{\bar{X}}_{\mathrm{u}}, \boldsymbol{\bar{X}}_{\mathrm{vt1}}]^\mathsf{T}$$

The augmented covariance matrix becomes the block diagonal of the UE, VT, and measurement covariances respectively.

$$\bar{P}_a = \text{blkdiag}(\bar{P}_u, \bar{P}_{vt1}, R)$$

The UKF functions by generating a set of sigma points $\bar{\gamma}_i$ and passing the sigma points through the nonlinear measurement model in order to estimate the state and covariance of the state. The sigma points are created using the unscented transform shown below:

$$\begin{split} \bar{\pmb{\gamma}}_0 &= \bar{\mathbf{X}}_{\mathrm{a}} \\ \bar{\pmb{\gamma}}_i &= \bar{\gamma}_0 + \bar{s}_i \sqrt{n_{\mathrm{x}} + n_{\mathrm{z}} + \lambda_u} \\ \bar{\pmb{\gamma}}_{i+n_{\mathrm{x}}+n_{\mathrm{z}}} &= \bar{\pmb{\gamma}}_0 - \bar{s}_i \sqrt{n_{\mathrm{x}} + n_{\mathrm{z}} + \lambda_u} \end{split}$$

where $i = 1, 2, \dots, n_x + n_z$ and \bar{s}_i is the i^{th} column of the Cholesky decomposition of \bar{P}_a . That is,

$$\bar{P}_a = \bar{S}\bar{S}^{\mathsf{H}}$$

where

$$\mathbf{\bar{S}} = [\bar{s}_1, \bar{s}_2, \cdots, \bar{s}_{n_x+n_z}]$$

The parameter λ_u is a tuning parameter that determines the distance from the mean the unscented transform explores. The value of λ_u is a function of the size of the augmented state n_x , measurements n_z , and the tuning parameters κ and α :

$$\lambda_{\rm u} = \alpha^2 \cdot (n_{\rm x} + n_{\rm z} + \kappa) - (n_{\rm x} + n_{\rm z})$$

where the tuning parameters are typically set to $\kappa = 0$ and $\alpha = 0.001$. But different tuning parameters can be set to modify the extent of exploration. The sigma points are passed through the nonlinear measurement function h as shown below.

$$\bar{\mathbf{z}}_i = h[\bar{\mathbf{\gamma}}_i(1:n_x), \bar{\mathbf{\gamma}}_i(n_x+1:n_x+n_z)]$$

The predicted measurement then becomes the weighted sum of the sigma points passed through the measurement function.

$$\bar{\mathbf{z}} = \sum_{i=0}^{2(n_x + n_z)} W_i \bar{\mathbf{z}}_i$$

Similarly, the measurement covariance \bar{P}_{zz} and cross covariance P_{xz} are found as shown below.

$$\begin{split} & \bar{\boldsymbol{P}}_{\text{ZZ}} = \sum_{i=0}^{2(n_{\text{X}} + n_{\text{Z}})} W_i^c [\bar{\boldsymbol{z}}_i - \bar{\boldsymbol{z}}] [\bar{\boldsymbol{z}}_i - \bar{\boldsymbol{z}}]^{\mathsf{T}} \\ & \bar{\boldsymbol{P}}_{\text{XZ}} = \sum_{i=0}^{2(n_{\text{X}} + n_{\text{Z}})} W_i^c [\bar{\boldsymbol{\gamma}}_i (1:n_{\text{X}}) - \bar{\boldsymbol{X}}] [\bar{\boldsymbol{z}}_i - \bar{\boldsymbol{z}}]^{\mathsf{T}} \end{split}$$

where the weights are defined as:

$$W_{0} = \frac{\lambda_{u}}{(n_{x} + n_{z} + \lambda_{u})}$$

$$W_{0}^{c} = \frac{\lambda_{u}}{(n_{x} + n_{z} + \lambda_{u})} + 1 - \alpha^{2} + \beta$$

$$W_{i} = W_{i}^{c} = \frac{1}{2(n_{x} + n_{z} + \lambda_{u})}$$

The value of β is typically set to 2. The estimate of the combined UE and VT state can now be found using the LMMSE update step:

$$\hat{\mathbf{X}} = \bar{\mathbf{X}} + \mathbf{P}_{xz}\mathbf{P}_{zz}^{-1}[\mathbf{z} - \bar{\mathbf{z}}]$$
$$\mathbf{P} = \bar{\mathbf{P}} + \mathbf{P}_{xz}\mathbf{P}_{zz}^{-1}\mathbf{P}_{xz}^{\mathsf{T}}$$

For each prior hypothesis a new hypotheses for each possible combination of measurement and VT is generated. For each new hypothesis a joint UE and VT UKF measurement update is performed using the same method as shown in the above steps. The key difference is the a priori distribution of the known VTs is modeled as a Gaussian distribution with mean and covariance found from the time update step.

After a measurement update is performed on all the VT and UE combinations, the resulting set of hypotheses represent all the possible data associations (DA). The Bernoulli existence probability P_{bh} for each DA h can be found. When the measurement is applied the $P_{bh} = 1$ representing that the VT is detected and is considered certain to exist. If there is no measurement associated with the existence probability is updated according to the following:

$$P_{bh}(k+1) = \frac{P_{bh}(k)(1 - P_{d})}{(1 - P_{bh}(k)) + P_{bh}(k)(1 - P_{d})}$$

This will occur if there are more VTs in the state than measurements at a given timestep.

3. Data Association

Determining the correct DA is critical to precisely estimating the UE and VT positions. Each DA is scored using the likelihood of the DA being consistent with the prior states. In order to determine the likelihood of each DA the normalized innovation squared (NIS) metric is found from the innovations \mathbf{v} and the innovation covariance matrix \mathbf{S} where $\mathbf{S} = \mathbf{P}_{zz}$.

$$NIS = \mathbf{v}^{\mathsf{T}} \mathbf{S}^{-1} \mathbf{v}$$

The NIS is distributed as a chi-square distribution with n_z degrees of freedom allowing the likelihood \mathcal{L}_h of DA h of the NIS to be found from the chi-square probability distribution function.

$$\mathcal{L}_h(\text{NIS}|\mathbf{z}) = \boldsymbol{\chi}^2(\text{NIS}:n_z)$$

Each possible DA is assigned a weight equal to the likelihood of the NIS falling within the chi-square distribution. For all the existing DA the weight w_{hz} for DA h and measurement z is defined by the product of the NIS likelihood \mathcal{L}_h representing how likely the DA is and the Bernoulli probability P_{bh} representing the probability of the VT existing.

$$w_{hz} = \mathcal{L}_{h}P_{b}$$

The case when no measurement is assigned to a VT is considered a missed detection. The weight assigned to a hypothesis with a missed detection is the sum of the probability that the VT does not exist and the probability that the VT exists and was not detected:

$$w_{hz} = (1 - P_b) + (1 - P_d)P_b$$

In the case that the measurement represents a new detection of a previously unknown VT the weight is the sum of the birth probability P_B from the Poisson point process, and λ_c is the clutter weight.

$$w_z = \lambda_c + P_{\rm B}$$

After all the weights of the separate DAs are found a cost matrix is created to represent the combine cost of all the possible DA at time (k).

$$C(k) = \begin{bmatrix} w_{11} & w_{12} & \cdots & w_{1n_z} & | & w_1 & 0 & \cdots & 0 \\ w_{21} & w_{22} & \cdots & w_{2n_z} & | & 0 & w_2 & \cdots & 0 \\ \vdots & \vdots & \vdots & \vdots & | & \vdots & \vdots & \vdots & \vdots \\ w_{n_h 1} & w_{n_h 2} & \cdots & w_{n_h n_z} & | & 0 & \cdots & \cdots & w_{n_z} \end{bmatrix}$$

The best global hypothesis is the set of VT hypotheses with the minimum cost, where each measurement is used only once. The γ -best global hypotheses are found using Murty's algorithm [Murty, 1968] to solve the γ -best assignment problem.

4. Global Hypothesis Estimator

The γ -best minimal cost global hypotheses found from Murty's algorithm is combined into a single best estimate for the set of VT positions. The best estimate for the set of VTs is found in two parts. First, the cardinality of the set of VTs is calculated using the discrete Fourier transform [García-Fernández et al., 2018]. The cardinality distribution of a multi-Bernoulli RFS is the convolution of the cardinality distributions of its Bernoulli components [García-Fernández et al., 2018]. The MAP cardinality n^* is used to determine the best global hypothesis j^* based upon the hypothesis weights w for the i hypotheses in the global hypothesis and the Bernoulli existence probabilities p as shown in the equation [García-Fernández et al., 2018] below:

$$j^* = \operatorname{argmax}_j \prod_{l=1}^{n^*} w_{j,i_l} p_{j,i_l} \prod_{l=n^*+1}^{n} w_{j,i_l} (1 - p_{j,i_l})$$

The best global hypothesis j^* at time k represents the single best data association at time k.

5. Joint State Estimator

The joint UE VT state is estimated using the best DA found from the best global hypothesis. In this step a UKF measurement update is performed over an augmented state containing the UE state and the set of VTs shown below.

$$\boldsymbol{\bar{X}}_{aug} = [\boldsymbol{\bar{X}}_{u}, \boldsymbol{\bar{X}}_{vt1}, \boldsymbol{\bar{X}}_{vt2}, \cdots, \boldsymbol{\bar{X}}_{vtn}]^{\mathsf{T}}$$

The augmented covariance becomes the block diagonal of the UE and VT covariance matrices.

$$\pmb{\bar{P}}_{aug} = \texttt{blkdiag}(\pmb{\bar{P}}_{u}, \pmb{\bar{P}}_{vt1}, \pmb{\bar{P}}_{vt2}, \cdots, \pmb{\bar{P}}_{vtn})$$

The state is then updated by performing a standard UKF measurement update, shown in Sec. IV.2, for the entire augmented state.

6. Hypothesis Pruning

At each timestep a new global hypothesis is created for each of the prior hypothesis and measurement combinations. In order to prevent the number of hypotheses from growing exponentially hypothesis pruning is performed. The pruning process first removes any VT estimates with a Bernoulli component equal to zero, which would represent a VT that is known to not exist. If there are multiple global hypotheses that are the same after removing the all the zero Bernoulli components, the global hypotheses are considered to represent the same hypothesis and their weights are combined. The global hypotheses are then sorted by weight and only the γ highest weighed global hypotheses are saved with all other hypotheses being removed. The number of global hypotheses γ is a tuning parameter of the UPMBM-SLAM filter which allows for a trade-off between processing time and estimation precision.

In the extreme case when γ is very large, there will be a large number of global hypotheses being saved at each timestep allowing for DA errors made far in the past to be corrected. The cost of having such a large γ is each hypothesis is required to be propagated each timestep requiring a large amount of computation as well as memory to store all γ hypotheses. In the case that $\gamma = 1$ only a single hypothesis is saved each timestep allow for fast computation time at the cost of the inability to correct any DA errors.

7. Map Optimization

After the UE has reached the end of its trajectory a map optimization is performed over the time history of detected VTs. Assuming the UPMBM-SLAM filter has converged the errors in the estimated VT locations will be approximately zero mean and Gaussian. The set of VTs is unlabeled requiring a k-means clustering operation to be performed to label the VT estimates so that each unique VT location can be optimized. The optimized map of VTs is found by performing a least squares estimate over each labeled set of VTs. The optimized map can be shared with all UEs in the same local area allowing them to warm start their respective UPMBM-SLAM estimators with a high confidence prior map.

8. Wall Detections

Measurements of the wall locations can be derived from the best estimate of the joint state. Each VT represents the image of the BS resulting from specular reflections off walls in the environment. The vector from the BS to the VT is normal to the plane of reflection. The plane of reflection passes through the vector at the midpoint of the vector. The point of specular reflection is the point where the vector from the VT to the UE passes through the plane of reflection as shown in Fig. 3. The wall detection is found by directly determining the point of intersection between the vector pointing from the UE to the VT and the plane of reflection.

V. SIMULATION PARAMETERS

The performance of the UPMBM-SLAM filter was validated using a dataset of simulated truth measurements from the Nova RF ray tracing software. Separate datasets were created for four UE trajectories in 4 separate environments with different wall layouts (Fig. 4). The truth dataset consists of the time of arrival, angle of arrival, and gain of each reflected signal for each UE trajectory. In each trajectory a single LOS BS with a known location is visible.

1. Measurement Simulation and Noise

The noisy measurements were created according to the measurement models shown in Sec. III.2. The pseudorange measurements are constructed using the true range between the BS and UE by multiplying the TOAs by the speed of light. Simulated clock offset $\delta t_n(k)$ for MPC n for timestep k and white Gaussian noise were added to the true range to build the pseudorange measurements. The AOA measurements were constructed according to the equations (3, 4) using the angle of arrival measurements directly from the Nova simulations. The measurement noise samples added to each of the AOA measurements are drawn from a Von Mises–Fisher distribution over a circle. The measurement errors variances were set to be $\sigma_\rho^2=1$ meter for the pseudorange error variance and $\sigma_\theta^2=\sigma_\phi^2=0.0875$ radians (5°) for the azimuth and elevation angle measurements, respectively. This represents the type of accuracy one could expect from a Mid-band 5G Positioning Reference Signals.

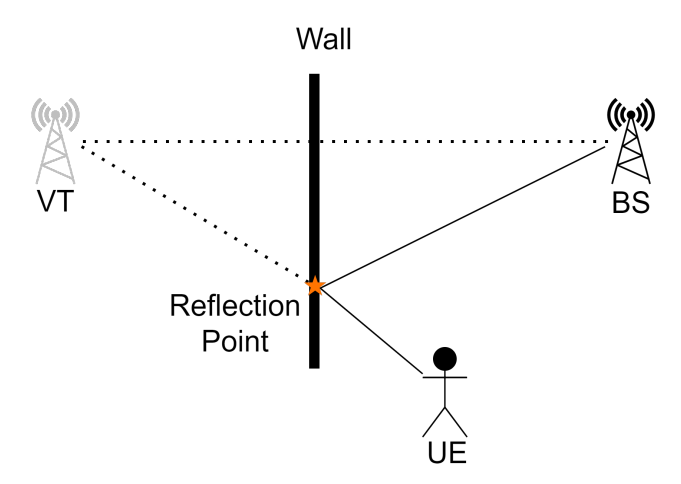


Figure 3: Sketch showing the relationship between the BS, VT, and specular reflection point. The location of the specular reflection can be calculated from the BS, VT, and UE positions if the position of the BS is known and the UE and VT can be estimated.

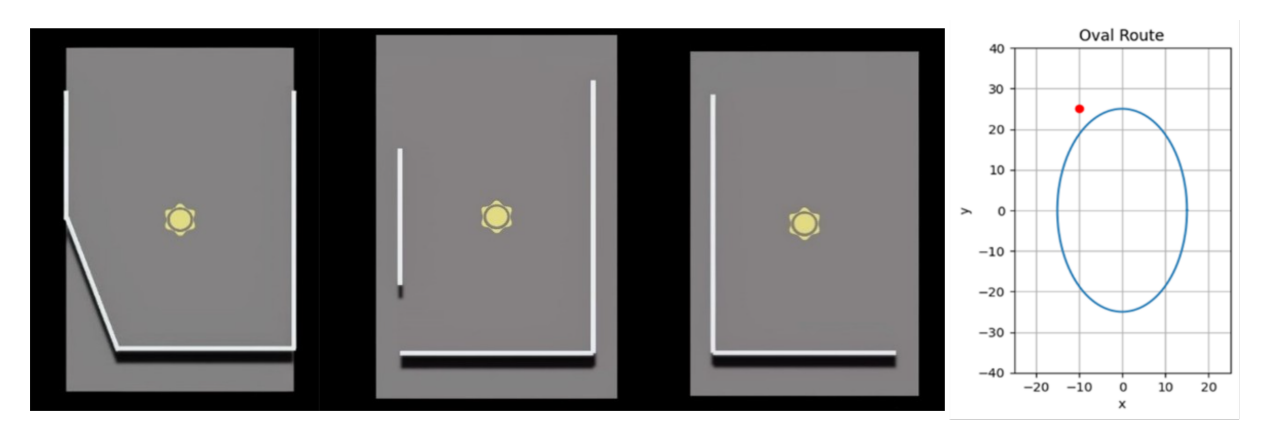


Figure 4: Simulated environments and paths used in the Nova RF ray tracing software. The first three images show the different environments tested and the walls that produce specular reflections. The last image shows the UE trajectories tested. The red dot shows the BS location.

Clutter measurements were added to the dataset at each timestep with the number of clutter elements being a Poisson random variable with mean λ . The value of each clutter measurement was generated by drawing a sample from a uniform distribution of pseudorange and AOA values over the observation area.

2. Clock Simulation

The simulated pseudorange measurements contain two additive components and noise. The first component is the Euclidean distance between the UE and the VT or BS, while the second component is the clock offset δt between the BS's clock and the UE clock. The clock offset is simulated with a first order simulation based on the two-parameter clock model presented in [Brown and Hwang, 2012]. The clock offset is simulated as a random walk in both phase and frequency. The first order random walk process can be simulated using the dynamics model shown below.

$$\begin{bmatrix} \delta t(k+1) \\ \delta \dot{t}(k+1) \end{bmatrix} = \begin{bmatrix} 1 & \Delta t \\ 0 & 1 \end{bmatrix} \begin{bmatrix} \delta t(k) \\ \delta \dot{t}(k) \end{bmatrix} + \mathbf{v}(k)$$

It is assumed that the UE clock is well characterized by the constant communication between the UE and the BS resulting in the constant clock rate δi is known to the UE clock and its effects can be subtracted from δt . The first order clock offset contains additive Gaussian noise v with the following covariance:

$$\mathbb{E}\left[\mathbf{v}\mathbf{v}^{\mathsf{T}}\right] = S_g \begin{bmatrix} \frac{\Delta t^3}{3} & \frac{\Delta t^2}{2} \\ \frac{\Delta t^2}{2} & \Delta t \end{bmatrix} + S_f \begin{bmatrix} \Delta t & 0 \\ 0 & 0 \end{bmatrix}$$

The covariance depends on the timestep Δt and the parameters S_g and S_f which define the stability of the clock. The parameters are defined as $S_g = 2\pi^2 h_{-2}$ and $S_f = \frac{h_0}{2}$ where the h_0 and h_{-2} parameters are found from the Allan deviation of a TCXO quality clock [Brown and Hwang, 2012].

3. IMU Simulation

The IMU measurements used to propagate the dynamics were simulated according to the true trajectory of the UE. The specific force measurements used to create the augmented UE state are generated as:

$$\ddot{\boldsymbol{x}}(k) = \boldsymbol{a}(k) + \boldsymbol{b}_a(k) + \boldsymbol{v}_a(k)$$

The simulation assumes that the orientation of the UE is aligned with the reference frame of the IMU allowing the specific force measurements \ddot{x} to be only a function of the true acceleration a, accelerometer bias b_a , and noise v_a . The accelerometer is assumed to be well calibrated allowing the bias term to be removed subtracted from the model when generating measurements. The noise term v_a is generated as Gaussian noise with covariance matrix:

$$Q_a = \left(\frac{9.8}{1000}\right)^2 \left(\frac{S_a}{\Delta t}\right) \mathbb{I}^{3x3}$$

The parameter S_a is defined as the accelerometer noise from the IMU specification sheet in $\frac{(mg)^2}{Hz}$. In this simulation the IMU parameters were selected to be consistent with consumer grade IMUs used in smartphones. For each timestep in the trajectory a noisy specific force measurement was simulated allowing the estimator to be evaluated under more realistic conditions.

VI. RESULTS

This section shows the results of running the UPMBM-SLAM estimator on the datasets of simulated measurements. This section is broken up into two parts. The first section demonstrates the performance of the UPMBM-SLAM estimator on a select single runs from the dataset. The second section demonstrates the effect of collaborative mapping by initializing the UPMBM-SLAM estimator with maps produced by different UEs in the same environment.

1. Single Run

The UPMBM-SLAM estimator was evaluated in the four-wall environment (Fig. 4) with the oval trajectory because it contains a short wall which caused one of the VTs to be visible for a short portion of the trajectory. This evaluated the estimator's ability to detect and track new VTs and demonstrated the ability to correctly assign the measurements to the correct VTs. The time history of the UE position (Fig. 4) shows the ability to track the UE's trajectory with VTs that appear and disappear. The results show the position of the UE can be estimated with a mean absolute position error of 3.02 meters. The main source of the error is in the z direction (Fig. 5) while the x and y position were estimated with sub-meter precision. The large z error is due to the large distance between the UE and VTs. As the separation between the UE and VTs increases the elevation angle approaches zero for any VT height and the larger the distance between the UE and VT the greater the impact of elevation angle noise on the height estimate.

The mapping performance was evaluated using the root-mean-square generalized optimal sub-pattern assignment (RMS-GOSPA) metric which determines how closely the estimated set of VTs matches the true set by comparing both the localization as well as missed detections and false detections. The results demonstrated that the UPMBM-SLAM estimator can determine the VT locations with an RMS GOSPA error of approximately 2.75 meters at the end of the trajectory (Fig. 5). It is noted that the mapping error increases around 200 seconds into the trajectory when a new VT becomes visible for the first time and slowly converges due to the low precision in the angular measurements. This allowed the measurements to be more easily assigned to the incorrect VT which can be seen as the large cloud of VT estimates around the left most VT in Fig. 4.

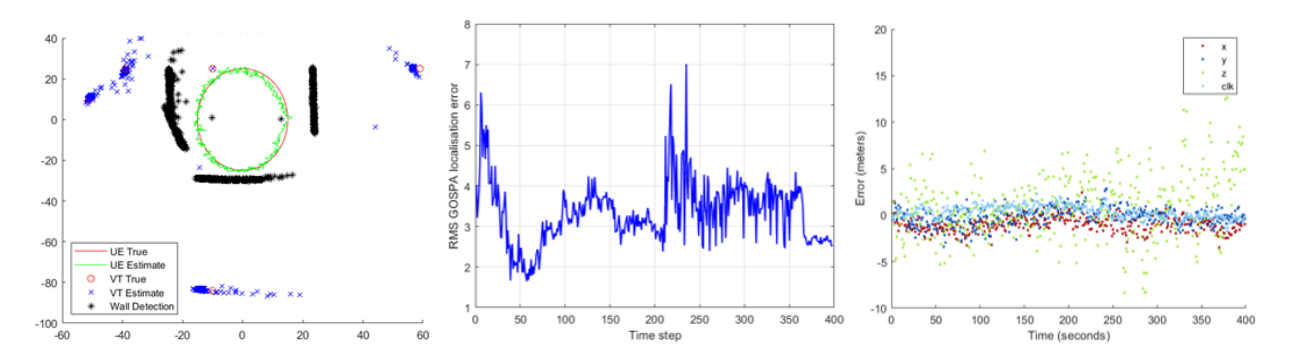


Figure 5: The left most figure shows the time history of the UE position estimate in green, the true UE trajectory in red, the VT position estimates in blue and the true VT positions as red circles. The black asterisks represent the wall detections. The time history of the RMS GOSPA error in the center shows the overall error in the map produced during the experiment. The mapping error slowly converges to approximately 2.75 meters RMS for the VT positions. The spike around 200 seconds shows the point when a new VT becomes visible, and its position must be estimated. The image on the right shows the time history of the position and clock errors during the experiment.

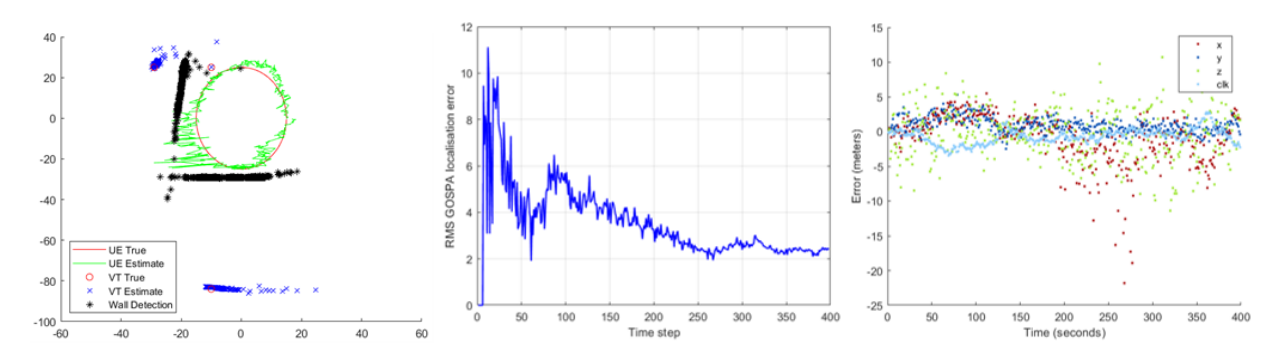


Figure 6: The right most figure shows the time history of the UE position estimate in green, the true UE trajectory in red, the VT position estimates in blue and the true VT positions as red circles. The black asterisks represent the wall detections. The time history of the RMS GOSPA error in the center shows the overall error in the map produced during the experiment. The mapping error slowly converges to approximately 2 meters RMS for the VT positions. The image on the right shows the time history of the position and clock errors during the experiment.

The effects of a reduced number of VTs were analyzed with an experiment performed in an environment with only two walls. The reduced number of VTs has a detrimental effect on the precision of the UE estimate. The lower performance is shown in demonstrated in Fig. 5 with the large deviations from the true trajectory. As a result, the mean absolute position error increased to 3.95 meters over the course of the trajectory. The map converges much quickly due to the lower number of VTs and results in an RMS GOSPA above 2 meters (Fig. 6).

2. Collaborative Mapping

The second component of the UPMBM-SLAM estimator is the ability to utilize multiple datasets of different UEs in the same environment. The collaborative mapping performance was evaluated by running the UPMBM-SLAM estimator sequentially on each of the four trajectories (Fig. 2). After each run the map was optimized and used to initialize the UPMBM-SLAM estimator for the next UE trajectory. The collaborative mapping allowed each subsequent UE to benefit from the prior VT map and refine the VT position estimates with new measurements. The sequential refinement of the VT map resulted in low covariance estimates for the VT positions for the final UE (Fig. 6). The errors in the UE state became nearly zero mean with a lower variance (Fig. 7) compared to the prior single run experiment. This resulted in an overall mean absolute position error of 2.80 meters with the x, y, z and clock offset mean absolute errors being 0.885, 0.677, 2.305, and 0.553 meters respectively. Similar to the prior experiment the largest source of position error was the estimate of the z position, and this was due to the high noise variance of the elevation angle measurements. The RMS-GOSPA of the VT map was also lower in this experiment and converged to a mean of approximately 1.5 meters (Fig. 7). This experiment demonstrates the UPMBM-SLAM estimator's ability to collaboratively build maps that multiple UEs can leverage for improved positioning performance while continuing to refine the VT map.

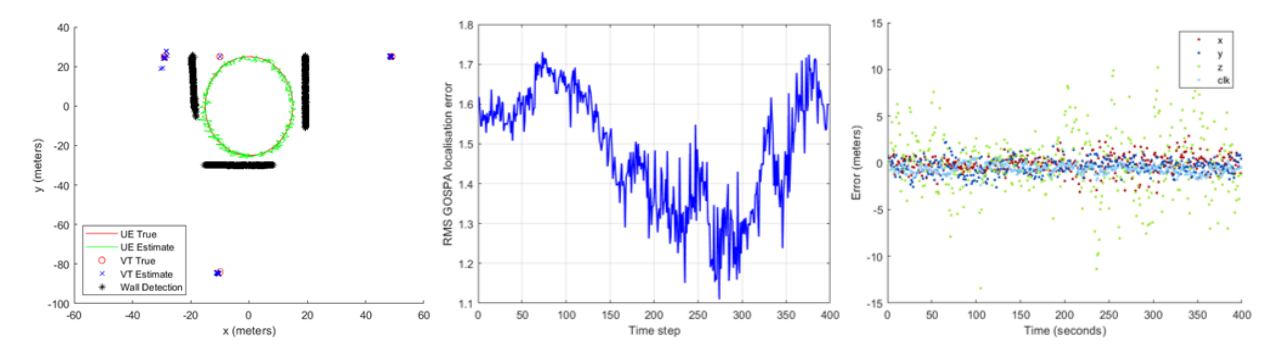


Figure 7: The right most figure shows the time history of the UE position estimate in green, the true UE trajectory in red, the VT position estimates in blue and the true VT positions as red circles. The black asterisks represent the wall detections. The time history of the RMS GOSPA error in the center shows the overall error in the map produced during the experiment. The mapping error has already converged to a steady state. The image on the right shows the time history of the position and clock errors during the experiment.

VII. CONCLUSIONS

This paper outlined the development of the UPMBM-SLAM estimator by tightly coupling an IMU with a UKF based PMBM filter and analyzed its performance. The performance of the estimator was tested using a dataset of simulated signal parameters from the Nova RF ray tracing software. The initial results of UPMBM-SLAM estimator performance demonstrated its ability to solve the RF-SLAM problem and produce a position solution with sub-meter precision in the x and y direction and a 3-meter position solution in z for a UE. The results also demonstrated the ability to create a map of VTs which can be generated collaboratively with data from multiple UEs.

ACKNOWLEDGMENTS

Research was sponsored by affiliates of the 6G@UT center within the Wireless Networking and Communications Group at The University of Texas at Austin.

REFERENCES

[Brown and Hwang, 2012] Brown, R. G. and Hwang, P. Y. (2012). *Introduction to Random Signals and Applied Kalman Filtering*. Wiley.

[Dwivedi et al., 2021] Dwivedi, S., Shreevastav, R., Munier, F., Nygren, J., Siomina, I., Lyazidi, Y., Shrestha, D., Lindmark, G., Ernström, P., Stare, E., et al. (2021). Positioning in 5G networks. *IEEE Communications Magazine*, 59(11):38–44.

[Gao et al., 2022] Gao, K., Wang, H., Lv, H., and Liu, W. (2022). Toward 5G NR high-precision indoor positioning via channel frequency response: A new paradigm and dataset generation method. *IEEE Journal on Selected Areas in Communications*, 40(7):2233–2247.

[García-Fernández et al., 2018] García-Fernández, Á. F., Williams, J. L., Granström, K., and Svensson, L. (2018). Poisson multi-Bernoulli mixture filter: Direct derivation and implementation. *IEEE Transactions on Aerospace and Electronic Systems*, 54(4):1883–1901.

[García-Fernández et al., 2021] García-Fernández, Á. F., Williams, J. L., Svensson, L., and Xia, Y. (2021). A poisson multi-Bernoulli mixture filter for coexisting point and extended targets. *IEEE Transactions on Signal Processing*, 69:2600–2610.

[Ge et al., 2022] Ge, Y., Kaltiokallio, O., Kim, H., Jiang, F., Talvitie, J., Valkama, M., Svensson, L., Kim, S., and Wymeersch, H. (2022). A computationally efficient EK-PMBM filter for bistatic mmWave radio SLAM. *IEEE Journal on Selected Areas in Communications*, 40(7):2179–2192.

[Gentner et al., 2016] Gentner, C., Ma, B., Ulmschneider, M., Jost, T., and Dammann, A. (2016). Simultaneous localization and mapping in multipath environments. In 2016 IEEE/ION Position, Location and Navigation Symposium (PLANS), pages 807–815. IEEE.

[Humphreys et al., 2020] Humphreys, T. E., Kor, R. X. T., and Iannucci, P. A. (2020). Open-world virtual reality headset tracking. In *Proceedings of the ION GNSS+ Meeting*, Online.

- [Kim et al., 2023] Kim, H., García-Fernández, A. F., Ge, Y., Xia, Y., Svensson, L., and Wymeersch, H. (2023). Set-type belief propagation with applications to mapping, MTT, SLAM, and SLAT. *arXiv e-prints*, pages arXiv–2305.
- [Kim et al., 2022] Kim, H., Granström, K., Svensson, L., Kim, S., and Wymeersch, H. (2022). PMBM-based SLAM filters in 5G mmWave vehicular networks. *IEEE Transactions on Vehicular Technology*, 71(8):8646–8661.
- [Koivisto et al., 2017] Koivisto, M., Hakkarainen, A., Costa, M., Kela, P., Leppanen, K., and Valkama, M. (2017). High-efficiency device positioning and location-aware communications in dense 5G networks. *IEEE Communications Magazine*, 55(8):188–195.
- [Leitinger et al., 2019] Leitinger, E., Meyer, F., Hlawatsch, F., Witrisal, K., Tufvesson, F., and Win, M. Z. (2019). A belief propagation algorithm for multipath-based SLAM. *IEEE transactions on wireless communications*, 18(12):5613–5629.
- [Murty, 1968] Murty, K. G. (1968). An algorithm for ranking all the assignments in order of increasing cost. *Operations research*, 16(3):682–687.
- [Ruffini et al., 2021] Ruffini, S., Johansson, M., Pohlman, B., and Sandgren, M. (2021). 5g synchronization requirements and solutions ericsson.
- [Tenny et al., 2023] Tenny, R. M., Sun, L. C., Duru, A., and Humphreys, T. E. (2023). Robust absolute headset tracking for extended reality. In *Proceedings of the IEEE/ION PLANS Meeting*, Monterey, CA.
- [Wu et al., 2022] Wu, Y., Wang, Y., Huang, J., Wang, C.-X., and Huang, C. (2022). A weighted random forest based positioning algorithm for 6G indoor communications. In 2022 IEEE 96th Vehicular Technology Conference (VTC2022-Fall), pages 1–6. IEEE.
- [Wymeersch et al., 2017] Wymeersch, H., Seco-Granados, G., Destino, G., Dardari, D., and Tufvesson, F. (2017). 5G mmWave positioning for vehicular networks. *IEEE Wireless Communications*, 24(6):80–86.
- [Yang et al., 2022] Yang, C., Mao, S., and Wang, X. (2022). An overview of 3GPP positioning standards. *GetMobile: Mobile Computing and Communications*, 26(1):9–13.
- [Yang et al., 2021] Yang, J., Wen, C.-K., Jin, S., and Li, X. (2021). Enabling plug-and-play and crowdsourcing SLAM in wireless communication systems. *IEEE Transactions on Wireless Communications*, 21(3):1453–1468.